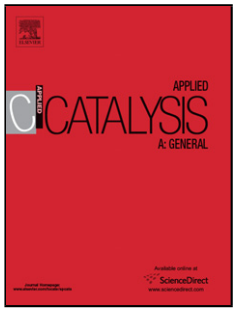

Title: Graphite encapsulated molybdenum carbide core/shell nanocomposite for highly selective conversion of guaiacol to phenolic compounds in methanol

Author: Rui Li Abolghasem Shahbazi Lijun Wang Bo Zhang Albert M. Hung David C. Dayton

PII: S0926-860X(16)30480-X
DOI: http://dx.doi.org/doi:10.1016/j.apcata.2016.09.016
Reference: APCATA 16012

To appear in: *Applied Catalysis A: General*

Received date: 19-7-2016
Revised date: 23-9-2016
Accepted date: 26-9-2016

Please cite this article as: Rui Li, Abolghasem Shahbazi, Lijun Wang, Bo Zhang, Albert M.Hung, David C.Dayton, Graphite encapsulated molybdenum carbide core/shell nanocomposite for highly selective conversion of guaiacol to phenolic compounds in methanol, Applied Catalysis A, General http://dx.doi.org/10.1016/j.apcata.2016.09.016

Graphite encapsulated molybdenum carbide core/shell nanocomposite for highly selective conversion of guaiacol to phenolic compounds in methanol

Rui Li[a], *Abolghasem Shahbazi*[b]*, *Lijun Wang*[b], *Bo Zhang*[b], *Albert M. Hung*[a], *David C. Dayton*[c]

[a] Joint School of Nanoscience and Nanoengineering, North Carolina A & T State University, Greensboro, NC 27411, USA

[b] Biological Engineering Program, Department of Natural Resources and Environmental Design, North Carolina A & T State University, 1601 East Market Street, Greensboro, NC 27411

[c] Energy Technology Division, RTI International, 3040 East Cornwallis Road, Research Triangle Park, Durham, NC 27709

Graphical abstract

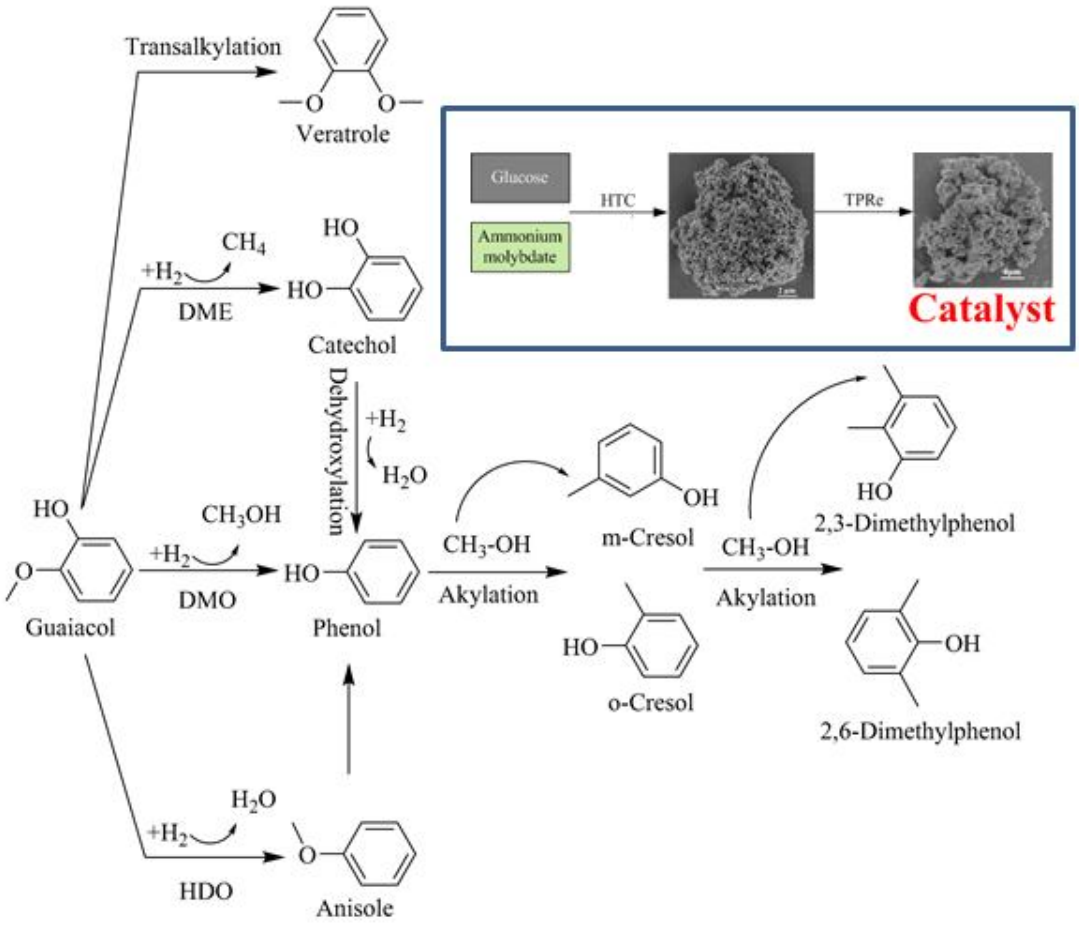

18

19

20 Highlights

21

22 1. The molybdenum core/graphite shell nanoparticles were synthesized by combining hydrothermal
23 carbonization and temperature programmed reduction.

24 2. The mechanism for the material formation is reported.

25 3. Highly selective conversion of guaiacol to phenolic compounds is achieved in alcohol.

26 4. Its reaction pathway is proposed.

27 5. Both demethoxylation (DMO) pathway and consecutive demethylation (DME) followed by a
28 dehydroxylation proceed concurrently to form phenol.

29

30

Abstract

Graphite encapsulated molybdenum carbides (Mo_2C@C) were synthesized *via* the hydrothermal carbonization of a solution of glucose and ammonium molybdate followed by temperature programmed reduction. Characterization and structural analyses revealed that the synthesized Mo_2C@C nanoparticles had a molybdenum core/carbon shell structure with a particle size ranging from 50 nm to 100 nm and a core size range of 5-45 nm. The catalytic performance of the graphite encapsulated molybdenum carbides was evaluated on conversion of guaiacol to phenolic compounds in methanol. At 340°C under 2.8 MPa hydrogen pressure, a 76.3% guaiacol conversion was obtained with selectivities of 68.6% for phenol and 93.5% for phenolic compounds. Thus, Mo_2C@C showed high selectivity for phenolic compounds in methanol.

Keywords: Encapsulation; Molybdenum carbides; Nanoparticles; Hydrothermal carbonization; Phenolic compounds

1. Introduction

Bio-oil produced from the pyrolysis of lignocellulosic biomass consists of a significant amount of phenolic compounds that were mainly derived from lignin [1]. The presence of these compounds with high oxygen contents leads to undesired properties for the bio-oil,

such as low heating value, thermal instability, high acidity, high viscosity, and incomplete volatility. Therefore, hydrodeoxygenation is often considered as a competitive route for upgrading bio-oil to transportation fuels or desired fine chemicals [2-5]. Guaiacol is one of the major phenolic compounds in pyrolytic bio-oil. Guaiacol has the greater propensity for coking than other phenolic compounds [6], and the complete deoxygenation is challenging due to its oxygenated hydroxyl and methoxy functional groups. Guaiacol was thus chosen as a model compound for the current study on the catalytic conversion of bio-oil components to desired chemicals.

The most widely studied catalysts for guaiacol hydrogenation are noble metal catalysts (such as supported Ru [7], Re [8], Rh [9, 10], Pd [7, 10], and Pt [11-14]) and molybdenum-based sulfide catalysts (such as sulfided CoMo [15-17] and NiMo [9, 18]), and the reaction schemes proposed in literature are summarized in Fig. 1. Noble metals are commonly presented as highly active hydrogenation catalysts. Noble metal catalysts could fully hydrogenate the guaiacol benzene ring, and then demethoxylate and dehydoxylate oxygenates to form saturated deoxygenated hydrocarbons, *e.g.* cyclohexanol and cyclohexane. Hydrogenation of guaiacol over Mo-based sulfide catalysts starts with demethylation and demethoxylation, which is followed by the benzene ring saturation to form major products such as catechol, phenol, benzene, and cyclohexane. Both noble metals and sulfide catalysts have their own shortcomings. For example, the use of noble metal produces completely saturated hydrocarbons, resulting in undesired H_2 consumption; while sulfide catalysts can be deactivated easily without sulfur addition [19]. Hydrogenation catalysts for phenolic compounds should have high activities towards selected products without causing saturation of the double bonds. Recently, molybdenum

carbide catalysts showed promising performances in many reactions involving hydrogen, including isomerization [20], hydrogenation [21-23], hydrodesulfurization [24-26], hydrodenitrogenation [27], and deoxygenation [28, 29]. Simultaneously, they exhibited good activity and selectivity in C–O/C=O bond cleavage [28, 30, 31], leading to dominant products with unsaturated C=C bonds rather than alkanes [32-34]. Therefore, molybdenum carbide was chosen as an efficient catalyst for the selective conversion of guaiacol to phenolic compounds.

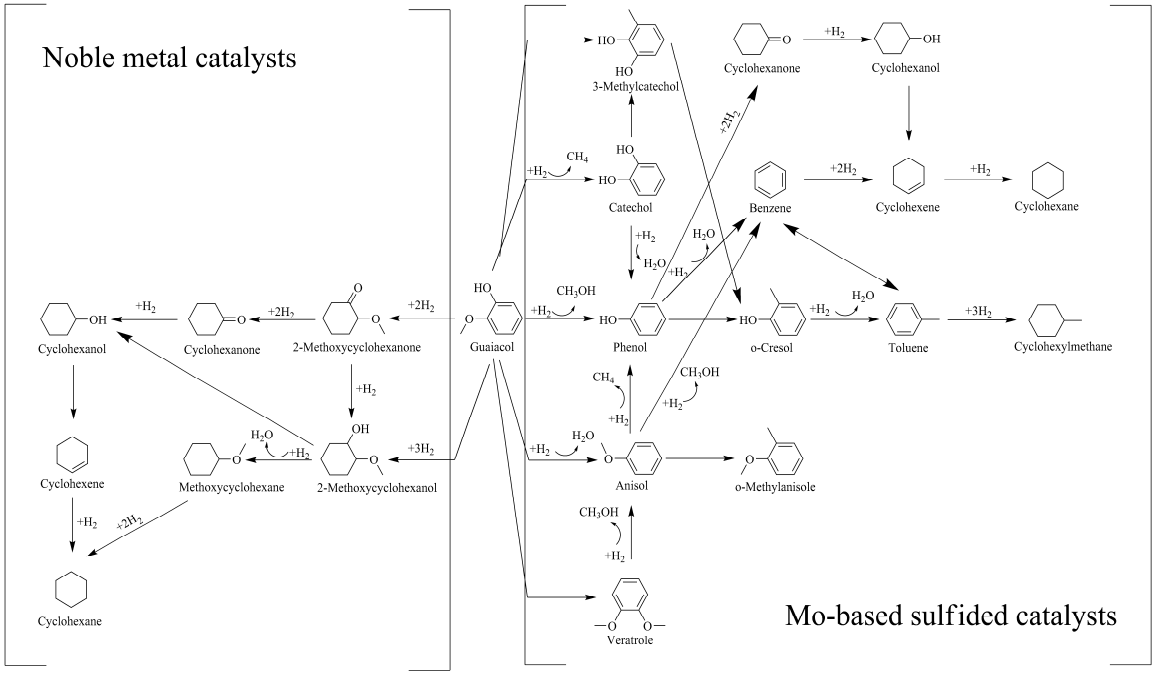

Figure 1. Reaction pathways for guaiacol hydrogenation over noble metal catalysts and Mo-based sulfide catalysts (according to ref. 3-14).

The conventional method for the synthesis of molybdenum carbides is temperature programmed reduction (TPRe) [35, 36]. The TPRe method involves gas-solid reactions between oxide or nitride precursors and a mixture of hydrogen and carbon-containing gas such as CH_4 [36-38], C_2H_4 [39], C_2H_6 [40], C_3H_8 [41, 42], C_4H_{10} [43], etc. Unfortunately,

high temperature during the TPRe process favors particle agglomeration, which makes it impossible to obtain a catalyst with nanoscale particles capable of potentially higher activities. In order to avoid the agglomeration of catalyst particles, one strategy is to prepare core/shell structure catalysts by using the hydrothermal carbonization (HTC) method. Hydrothermal carbonization has been employed successfully to synthesize carbonaceous spheres with controlled sizes from a solution of saccharides [44] and encapsulate metal nanoparticles in carbon nanospheres [45-49]. Through this method, homogeneously dispersed metal nanoparticles are encapsulated and isolated largely by permeable carbonaceous matrices that are generated in-situ [50].

Lignin is the only relevant renewable feedstock for aromatic compounds [51], but with low selectivity for specific compound [52]. In this study, carbon encapsulated molybdenum carbides were synthesized *via* a one-step hydrothermal carbonization followed by TPRe, and the catalyst activity was tested on conversion of guaiacol to phenolic compounds in methanol. The possible mechanism for the fabrication of this core/shell nanoparticle is proposed. The effects of temperature, pressure of hydrogen, and solvents on phenolic compounds production were investigated to elucidate the reaction pathway.

2. Experimental

2.1 Catalyst synthesis

Carbon encapsulated molybdenum carbides were prepared *via* hydrothermal carbonization of a solution of glucose and ammonium molybdate followed by temperature programmed reduction. A total of 0.0015 mol ammonium molybdate tetrahydrate

112 ($(NH_4)_6Mo_7O_{24}\cdot 4H_2O$, 99%, Sigma-Aldrich) and 0.132 mol glucose (96%, Sigma-Aldrich)
113 were dissolved in 600 mL deionized water. The solution was then treated hydrothermally
114 in an autoclave at 180°C for 8 h. The resultant precipitate was washed thoroughly with
115 deionized water and ethanol. The solid product was dried at 80°C. This hydrothermal
116 carbonization derived compound was denoted as MoO_2@C, in which MoO_2 represents
117 molybdenum oxide including molybdenum dioxide and molybdenum trioxide. The dried
118 MoO_2@C was further carbonized in 20 vol% CH_4 and 80 vol% H_2 at a flow rate of 50
119 mL/min. The carburization temperature was raised to 300°C at a heating rate of 5 °C/min
120 and then ramped to 900°C at a heating rate of 1 °C/min and kept at 900°C for 2 h. The
121 resulting material was then cooled down to room temperature in argon and subsequently
122 passivated under 1 vol% O_2 and 99 vol% N_2. The synthesized sample from the
123 carbonization process was denoted as Mo_2C@C.

124

125 **2.2 Catalyst characterization**

126 X-ray powder diffraction (XRD) patterns were obtained using an Agilent Gemini X-
127 ray Diffraction System (Santa Clara, CA, USA) operated at 40 kV and 40 mA with Cu-Kα
128 radiation. The morphology was examined on a JEOL JSM-7600F scanning electron
129 microscope (SEM) (Tokyo, Japan) operated at 2 kV with energy-dispersive X-ray
130 spectroscopy (EDX). Prior to the imaging, the sample was sputter-coated with 5 nm of
131 gold-palladium. High-resolution transmission electron microscopy (HRTEM) was
132 performed with a JEOL 2010F operated at 200 kV (Tokyo, Japan). Fourier Transform
133 Infrared (FT-IR) spectra were collected on a Varian 670 FT-IR spectrometer (Santa Clara,
134 CA, USA) equipped with a single-bounce diamond attenuated total reflectance accessory.

The amount of Mo in catalysts was measured using a Varian 710-ES inductively coupled plasma optical emission spectrometer (ICP-OES) (Santa Clara, CA, USA). The content of carbon and hydrogen were determined using a Perkin-Elmer 2400 CHN/S analyzer (Waltham, MA, USA). Thermogravimetric analyses (TGA) were performed using a TA SDT Q600 thermogravimetric analyzer (New Castle, DE, USA), in which samples were heated to 900ºC at a heating rate 10 ºC/min in nitrogen. Surface area and porosity were analyzed by measuring physical nitrogen adsorption using a Micromeritics ASAP 2020 (Norcross, GA, USA).

2.3 Catalytic tests

The catalytic performance of Mo_2C@C was evaluated in a 75 ml Parr stainless steel batch autoclave (St, Moline, IL, USA). A mixture of 0.2 mL guaiacol (98%, Sigma-Aldrich), 10 mL solvent methanol, 0.05 mL hexadecane (99%, Sigma-Aldrich) as the internal standard, and 0.1 g catalyst was loaded into the reactor vessel. The vessel was evacuated by pressurization-depressurization with nitrogen to purge out any air and then charged with hydrogen to a certain pressure. A higher initial hydrogen pressure of 2.8 MPa was used to ensure excess hydrogen supplement. The hydrotreating process proceeded at a given temperature for 4 h. Table S1 gives the experimental conditions. After the hydrotreatment, the liquid samples were analyzed by using an Agilent 7890A gas chromatograph (Santa Clara, CA, USA) equipped with a 5975C mass spectrometry (GC-MS), a flame ionization detector (FID), and a DB-1ms capillary column. Helium gas was used as carrier gas with a split ratio of 50:1. The GC oven was held at 35°C for 5 min, then ramped to 200°C at 5 °C/min.

The conversion was determined by averaging the data measured twice. The conversion efficiency and selectivity of guaiacol during hydrotreating were defined as:

$$\text{Guaiacol conversion (\%)} = \frac{N_{\text{guaiacol loaded}} - N_{\text{unconverted guaiacol}}}{N_{\text{guaiacol loaded}}} \times 100 \quad (1)$$

$$\text{Selectivity to specific product (\%)} = \frac{N_{\text{specific product}}}{N_{\text{guaiacol loaded}} - N_{\text{unconverted guaiacol}}} \times 100 \quad (2)$$

where "N" represents the moles of the reactants or products.

3. Results and discussion

3.1 Characterization of carbon encapsulated molybdenum oxide

Carbon encapsulated molybdenum oxide (MoO_2@C) was synthesized *via* hydrothermal carbonization of a solution of glucose and ammonium molybdate followed by drying at 80°C. XRD spectra showed that this synthesis method formed a poorly crystalline phase (Fig. 2a), which was assigned to hexagonal MoO_2 (PDF 50-0739) with 2θ peaks at 36.5° (1 0 0), 53.8° (1 0 2), 65.7° (1 1 0), and 41.4° (1 0 1). The carbonaceous phase in these samples was amorphous as no graphitic carbon peaks were observed. EDX analysis confirmed the exclusive existence of Mo, C, and O in the as-synthesized MoO_2@C. The Mo element was evenly distributed in MoO_2@C (supplementary information Fig.S1). The elemental analysis shows that the contents of C and Mo were 51.0 and 15.9 wt%, respectively. The BET surface area and total pore volume of the catalyst were 37.6 m^2/g and 0.25 cm^3/g, respectively. Morphological images of MoO_2@C exhibited a porous structure composed of numerous attached carbonaceous spheres with sizes ranging from

50 to 100 nm (Fig. 3a-3b). In Fig. 4a, the HRTEM shows that the catalyst had a core-shell structure with the molybdenum oxide encapsulated inside carbonaceous spheres during the hydrothermal carbonization treatment. Molybdenum oxide cores had a size distribution between 5 and 56 nm and were dispersed homogeneously in a carbonaceous matrix. The lattice spacing of 0.25 and 0.17 nm (Fig. 4b) could be assigned to the (1 0 0) and (1 0 2) planes of MoO_2. Fig. 5a shows the surface functional groups on the carbonaceous shells identified by FT-IR spectroscopy. The bands around 1615 cm^{-1} were attributed to in-plane C=C stretching vibration in an aromatic ring, and the band at 767 cm^{-1} was for aromatic C–H out-of-plane bending vibrations [53]. These characteristic absorptions of aromatic rings confirmed the aromatization of glucose during the hydrothermal treatment. The band at 1698 cm^{-1} was attributed to C=O vibration of aldehydes, ketones, carboxylic acids, or esters [48]. The broad band centered around 3400 cm^{-1} corresponded to O–H stretching vibration and 1292 cm^{-1} was from C–OH bending vibration, which implied the existence of hydroxyl groups. The bands at 2975 and 2934 cm^{-1} were stretching vibrations of aliphatic C–H, which showed that the carbonaceous shell also possessed an aliphatic structure. In summary, the dehydration and subsequent aromatization of glucose during hydrothermal treatment resulted in carbonaceous hydrophilic shells with abundant –OH and C=O groups.

3.2 Characterization of graphite encapsulated molybdenum carbide

Graphite encapsulated molybdenum carbide (Mo_2C@C) was synthesized through the process of the temperature programmed reduction at 900ºC under 20% CH_4/80% H_2. TPRe treatment resulted in the formation of hexagonal β-Mo_2C (PDF 35-0787) with 2θ peaks at

~39.4° (1 0 1), 38.0° (0 0 2), 52.1° (1 0 2), 34.4° (1 0 0), 61.7° (1 1 0), 69.6° (1 0 3), and 74.7° (1 1 2) (Fig. 2b). Besides the peaks of β-Mo_2C, the diffraction peaks at 26.1° (0 0 2), 42.7° (1 0 0), and 44.4° (1 0 1) confirmed the formation of graphite (PDF 41-1487). Clair et al. [54] and Hanif et al. [40] also observed a similar phenomenon that graphite was formed from methane at a temperature higher than 700°C. The TPRe treatment did not significantly change the morphology of Mo_2C@C and the size of carbonaceous shells for Mo_2C@C that was still in the range of 50-100 nm as shown in Fig. 3d. EDX analysis showed that Mo and C were evenly distributed in the sample (supplementary information Fig.S2). The HRTEM images indicated that the size of the molybdenum carbide cores was between 32 and 45 nm in Fig. 4c and between 5-15 nm in Fig. 4d, and the carbonaceous matrix effectively inhibited the agglomeration of the molybdenum nanoparticles. The lattice spacings of 0.23, 0.24, and 0.26 nm could be assigned to the (1 0 1), (0 0 2), and (1 0 0) planes of Mo_2C, respectively, while the lattice spacing of 0.34 nm could be assigned to the (0 0 2) plane of graphite. A multilayer graphite was found to be formed on the surface of molybdenum carbide particles in Fig. 4d. The BET surface area and the total pore volume of the synthesized material increased significantly from 37.6 m^2/g to 177.0 m^2/g and 0.25 cm^3/g to 0.34 cm^3/g, respectively, while the carbon content increased from 51.0 wt% to 55.7 wt% and the oxygen content decreased from 28.3 wt% to 12.7 wt% in Table 1. This core-shell structured porous material with large pore sizes acts as a physical barrier, but still allow reactants reach reactive sites and products flow freely through the pores, which is in agreement with the results reported in the literature [50]. FT-IR spectra of Mo_2C@C indicated that most of functional groups on the carbon surface of MoO_2@C were removed during the heat treatment. The hydroxyl bands at 3400 cm^{-1} and 1292 cm^{-1} were

not observed, indicating that dehydration occurred during carbonization. The disappearance of C=O at 1698 cm^{-1} was associated with the decomposition of carboxylic acids. The disappearance of the peak at 767 cm^{-1} and 1615 cm^{-1} was due to internal structural reorganizations of aromatic structures and the further carbonization of the shell during the heat treatment. Therefore, almost all the oxygen-containing functional groups on the surface were removed at 900°C. This process may also have resulted in the development of mesopores in the carbonaceous matrix of Mo_2C@C as evidenced by the significant increase in BET surface area. Newly developed pores would increase not only the surface area but also the penetration of reactive species for catalytic reactions.

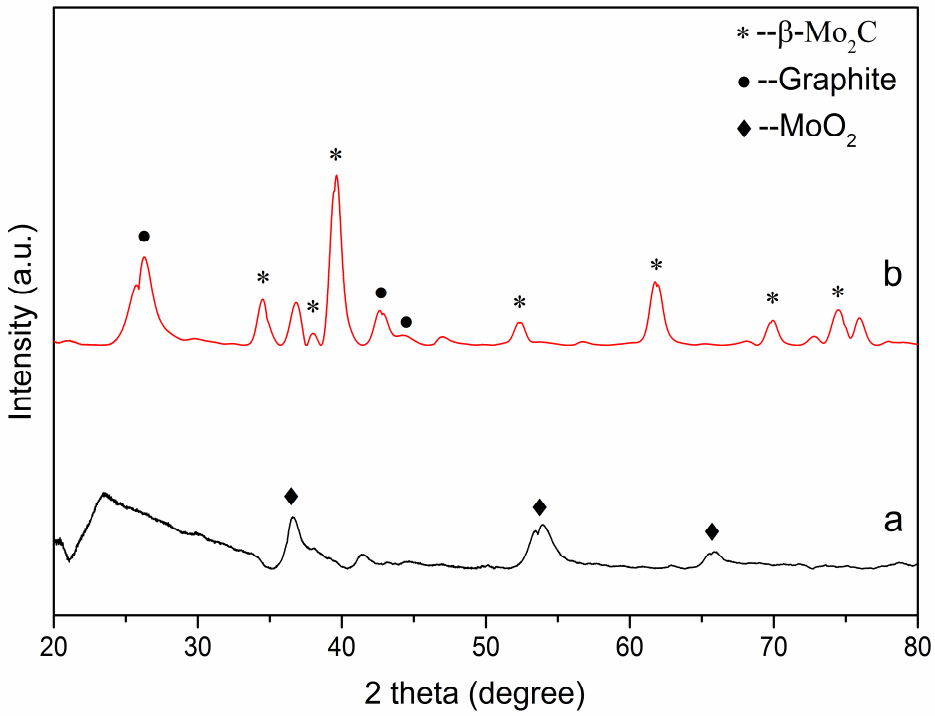

Figure 2. XRD patterns of (a) MoO_2@C, and (b) Mo_2C@C.

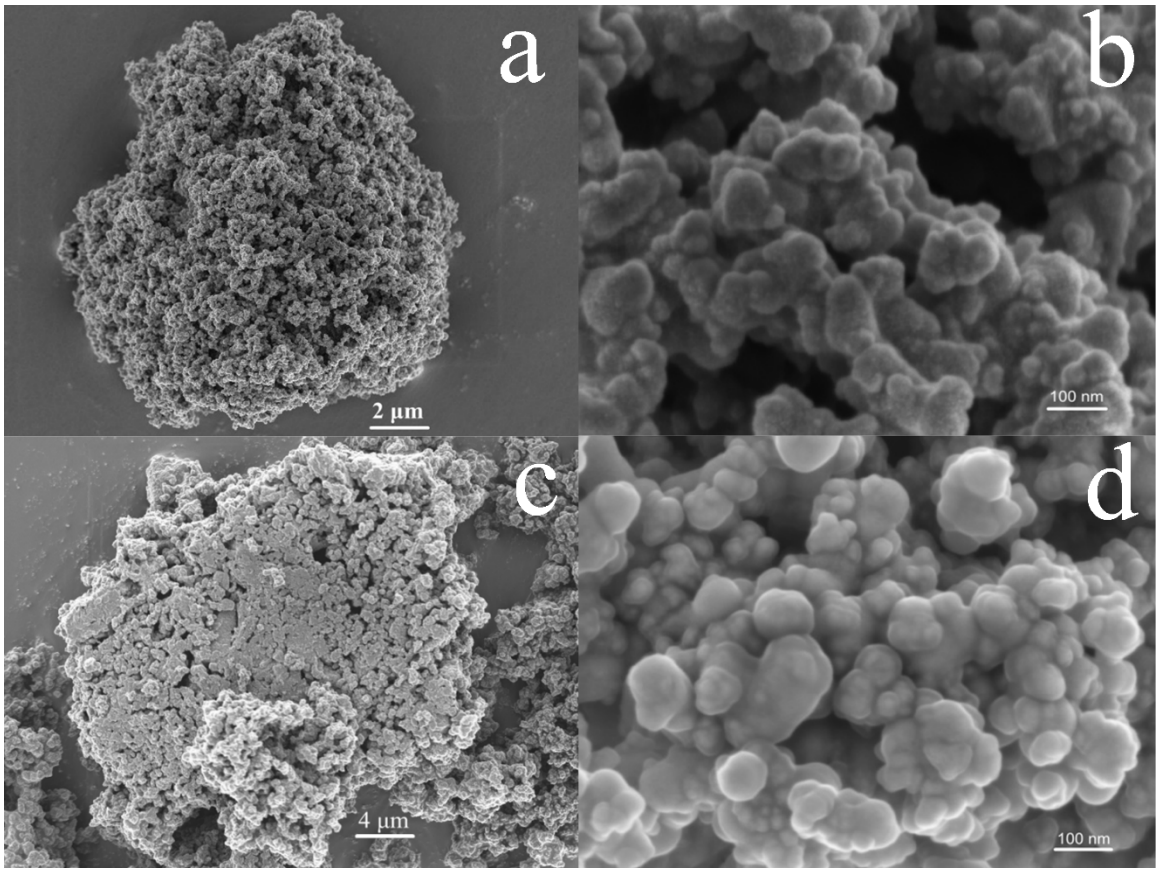

Figure 3. SEM images of (a, b) MoO_2@C, and (c, d) Mo_2C@C.

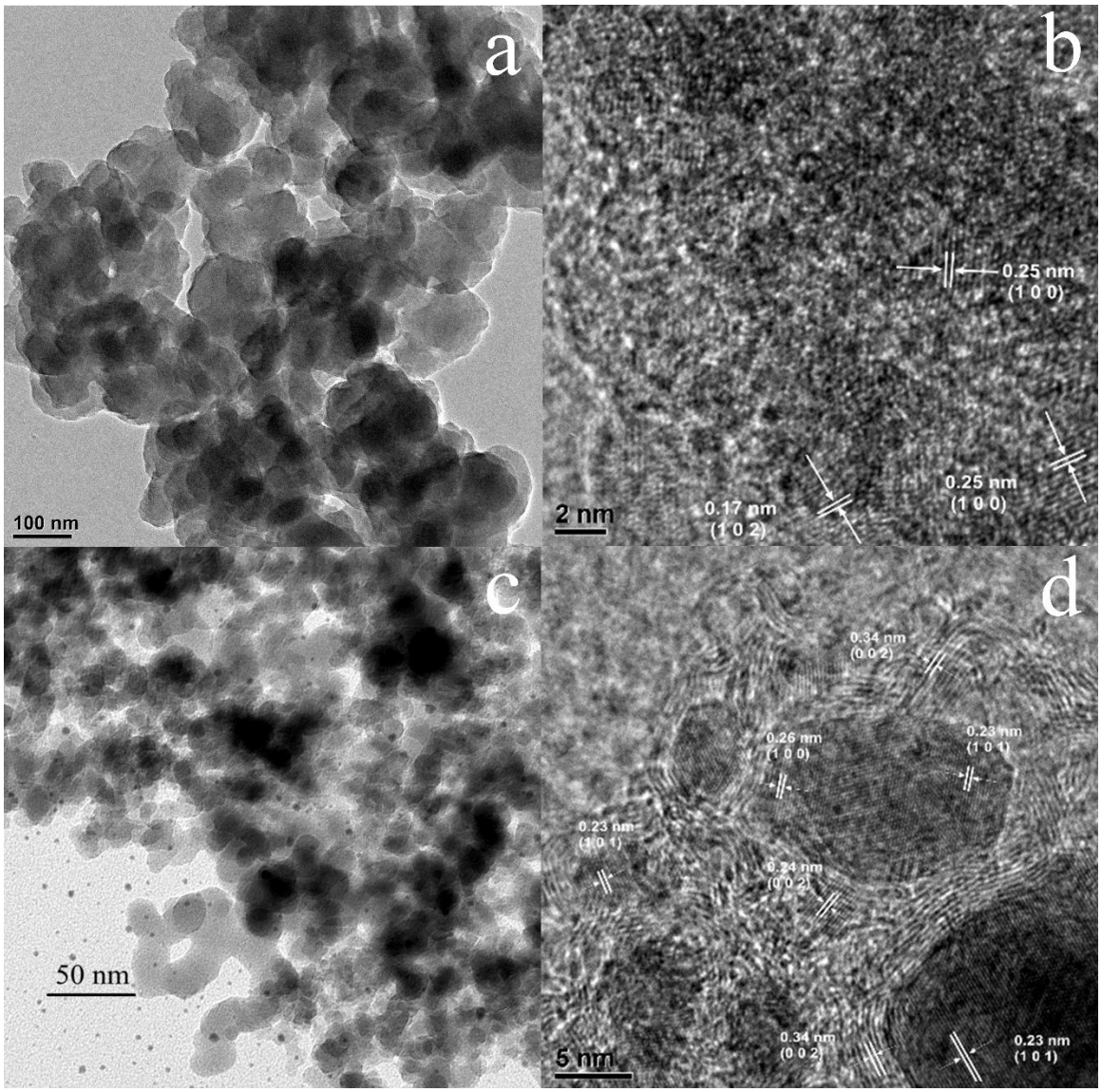

Figure 4. HRTEM images of (a, b) MoO_2@C, and (c, d) Mo_2C@C.

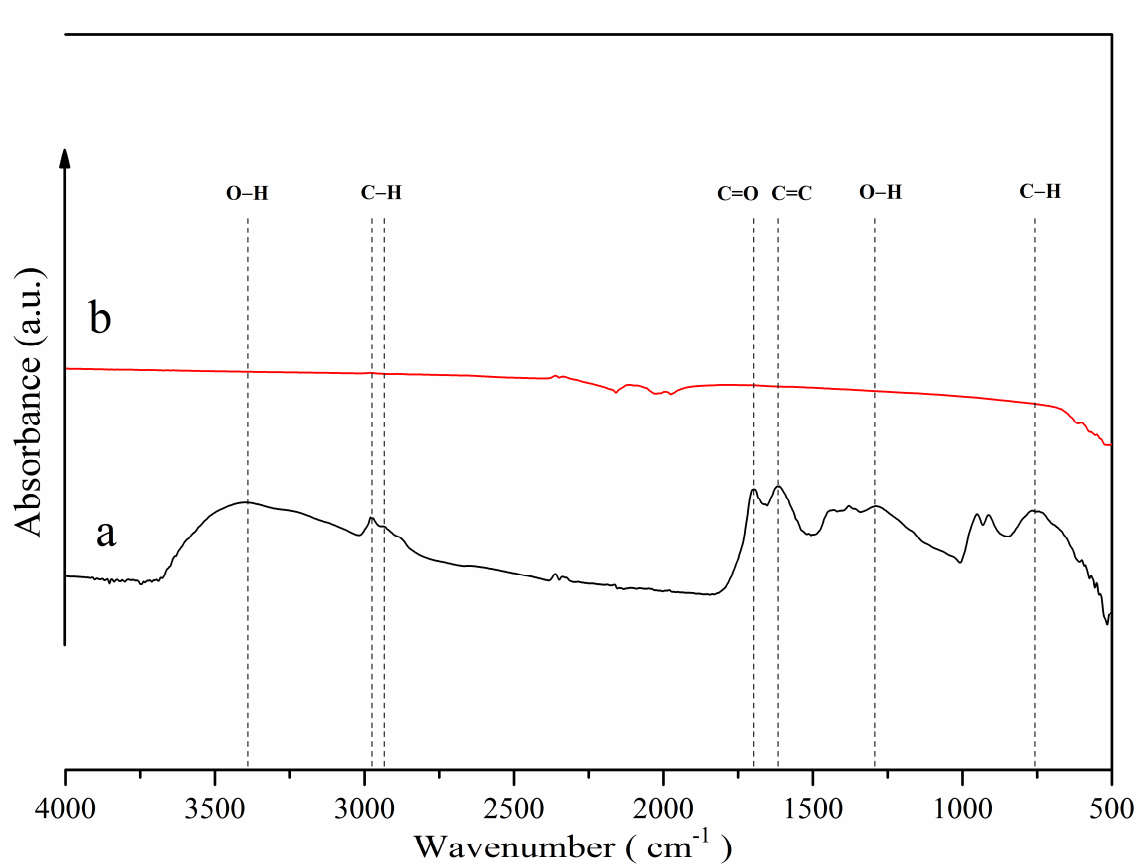

Figure 5. FT-IR spectra of (a) MoO_2@C, and (b) Mo_2C@C.

Table 1. Textural parameters of materials (on dry basis).

Sample	C[a] (wt%)	H[a] (wt%)	Mo[b] (wt%)	BET[c] ($m^2\ g^{-1}$)	Pore Diameter[d] (nm)	Pore Volume[e] ($cm^3\ g^{-1}$)
MoO_2@C	51.0	4.8	15.9	37.6	40.1	0.25
Mo_2C@C	55.7	4.7	26.9	177.0	31.4	0.34

[a] Measured with the Perkin-Elmer 2400 CHN/S analyzer.
[b] Measured with ICP
[c] Brunauer-Emmet-Teller (BET) surface area.
[d] Pore diameter calculated by the Barrett-Joyner-Halenda (BJH) method using adsorption branches.
[e] Total pore volume calculated from the amount of nitrogen adsorbed at a relative pressure of 0.995.

3.3 Mechanism for the formation of carbon encapsulated molybdenum nanoparticle

The mechanism of formation of carbon nanospheres prepared under hydrothermal conditions in the temperature range of 160-200 °C has been well summarized in studies [55-58]. However, the mechanism for the formation of metal oxide within carbonaceous spheres by one pot method is still under investigation. The interplay between the metal oxide and carbonaceous spheres and the precipitation kinetics of both phases are crucial to carbon encapsulated metal oxide formation [47]. Fig. 6 is a schematic illustration explaining the possible formation process of molybdenum nanoparticles encapsulated in carbon by in situ hydrothermal reduction of molybdenum ions with glucose based on our characterization results. At the initial stage, glucose is hydrolyzed to small carbonaceous colloids. Meanwhile, molybdenum is reduced from the oxidation state Mo^{6+} in $(NH_4)_6Mo_7O_{24}\cdot 4H_2O$ to Mo^{4+} in MoO_2 due to the ability of glucose degradation products to act as reductants [59]. The molybdenum nanoparticles combine with carbonaceous colloids through Coulombic interactions until condensing from water [45]. The further growth of carbon spheres *via* intermolecular dehydration of the surface functional groups follows the LaMer model [60]. Because homogeneous nucleation requires higher activation energy than heterogeneous nucleation [61], pure carbon nanospheres form at much lower rate than carbon encapsulated molybdenum oxide nanoparticles. All carbon encapsulated molybdenum oxide nanoparticles and pure carbon nanospheres interconnect randomly in three dimensions to form a hydrophilic microcomposite. During TPRe, molybdenum oxide reacts with methane and hydrogen to form hexagonal molybdenum carbide with a preserved structure, while graphite is formed on the surface of molybdenum carbide particles from methane.

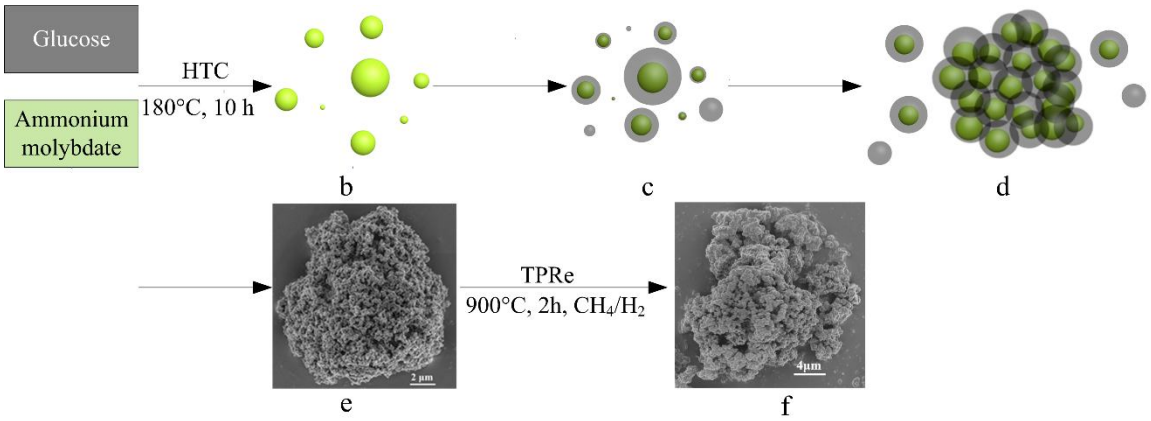

Figure 6. Schematic illustration for possible formation process for carbon encapsulated molybdenum particles.

(a) An aqueous solution of glucose and ammonium molybdate. (b) Molybdenum oxide (green dots) particles nucleate during HTC. (c) Molybdenum oxides (green core) are encapsulated in carbon shell (black shell) and carbonaceous colloids (black dots) formed. (d and e) The carbon encapsulated molybdenum oxides and carbon nanospheres randomly interconnect together to form a microcomposite. (f) Molybdenum carbides were synthesized by TPRe.

3.4 Catalytic performance of carbon encapsulated molybdenum carbide

The product profiles can be found in Table S2 of the supporting information. For comparison, the guaiacol conversion efficiencies in the absence of the catalyst at 340°C were 28.4% and 13.6% for the experiments with and without 2.8 MPa H_2, respectively. Fig. 7 shows the product yields obtained at reaction temperatures of 300°C, 320°C, and 340°C under a H_2 pressure of 2.8 MPa for 4 h. The increase of temperature from 300°C to 340°C increased the conversion efficiency of guaiacol from 32.5% to 76.3%, and the selectivities of phenol and phenolic compounds from 66.1% to 68.6% and 81.2% to 93.5%, respectively. The selectivity of catechol that is a reaction intermediate decreased with increasing

290 temperature, which means that more catechol was converted to phenol at a higher
291 temperature. After the reaction, H_2, CH_4, and CO_2 were detected in the gas phase.

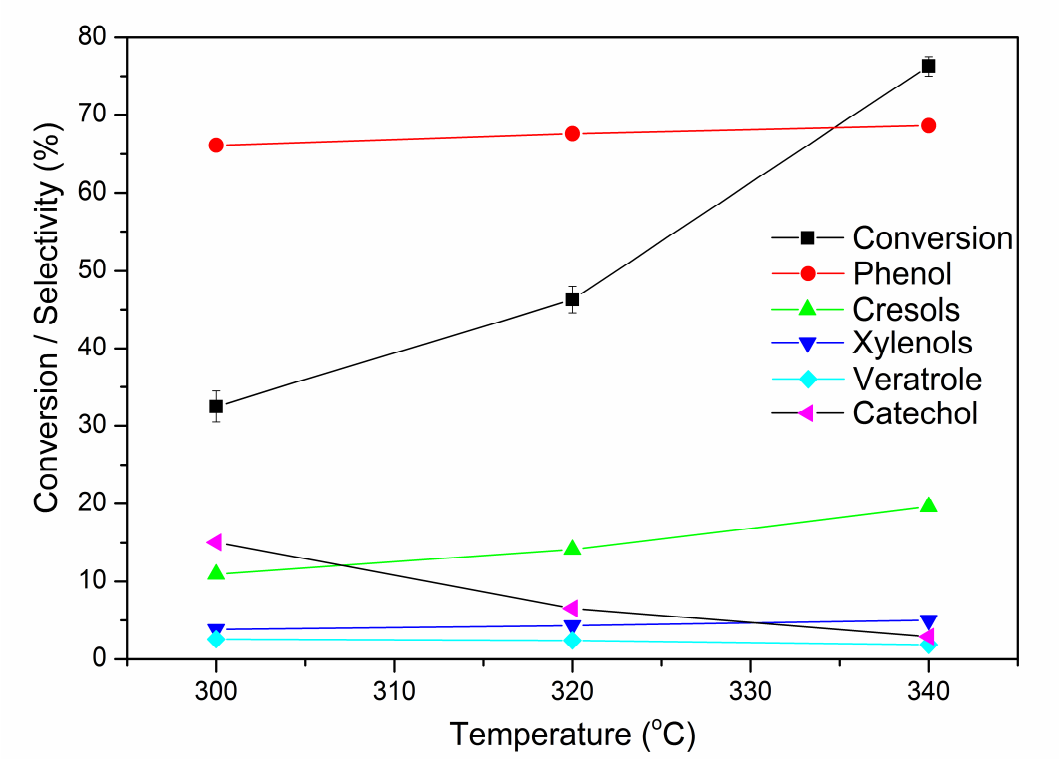

292

293 **Figure 7.** Conversion of guaiacol, and the selectivity to phenol, cresols, xylenols,
294 veratrole, and catechol over Mo_2C@C at temperatures of 300°C, 320°C, and 340°C.

295 As shown in Fig. 8, when the initial H_2 pressure was increased from 0.0 to 2.8 MPa,
296 the conversion efficiency of guaiacol increased from 50.9% to 76.3% and the phenolic
297 selectivity increased from 67.0 to 93.5%. In the absence of initial H_2, methanol also served
298 as a hydrogen donor. However, the selectivity towards phenol without H_2 was only half of
299 that of the process with H_2. High hydrogen pressures increased the selectivity for phenolic
300 compounds. Compared with the similar research [34], under the same reaction condition
301 (in methanol, at 340ºC, under 0 MPa H_2, for 4 h), the main products from guaiacol

conversion between two studies were the same. But the selectivity in this study is higher than that in the previous study.

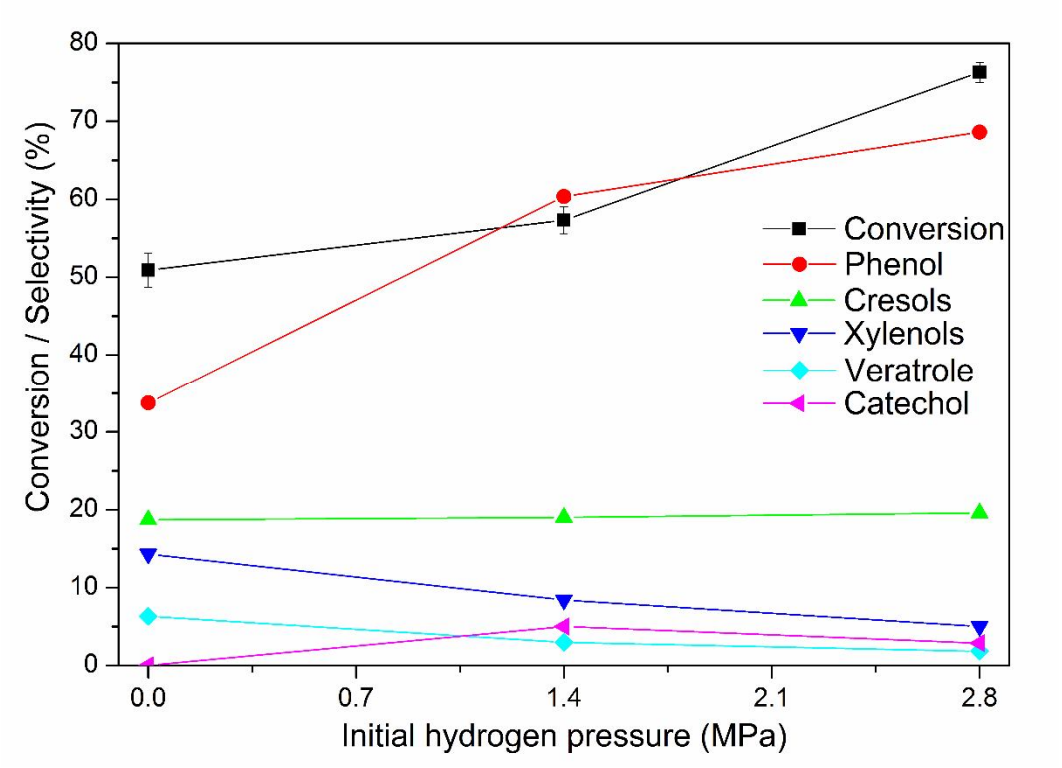

Figure 8. Conversion of guaiacol, and the selectivity to phenol, cresols, xylenols, veratrole, and catechol over Mo_2C@C at an initial H_2 pressure of 0, 1.4, and 2.8 MPa.

The reusability of the catalyst was evaluated at 340°C for 4 h in the methanol solvent for three cycles. A standard reaction was first performed on a freshly prepared Mo_2C@C catalyst. After each cycle, the spent catalyst was retrieved, dried at 105°C overnight, and reused directly in the next run without reactivation. As shown in Fig. 9, the conversion of guaiacol decreased slightly from 76.3% for the first cycle to 62.9% for the third cycle, while the selectivity towards phenol decreased from 68.6% to 64.1% and phenolic compounds decreased from 93.5% to 90.8%.

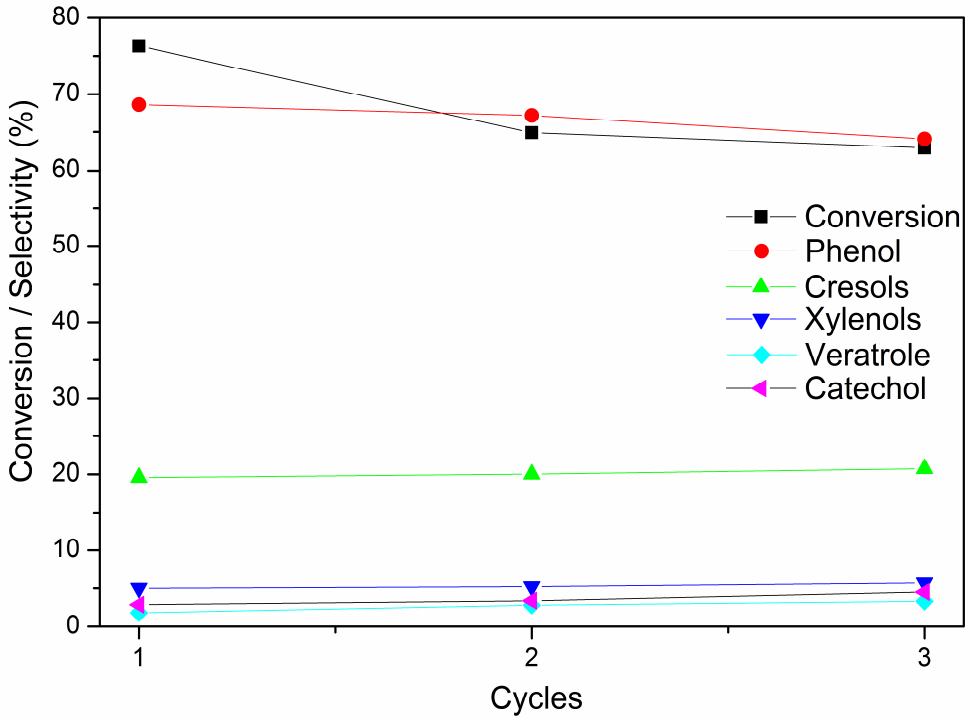

Figure 9. Conversion of guaiacol, and the selectivity to phenol, cresols, xylenols, veratrole, and catechol over recycled Mo_2C@C.

3.5 Reaction pathway for phenolic compounds production over Mo_2C@C

The product profiles showed that the selectivities towards phenol, cresols (o-Cresol, and m-Cresol), and xylenols (2, 3-dimethylphenol and 2, 6-dimethylphenol) were high. Trace amounts of veratrole, catechol, and anisole were also measured, but other transalkylation products were not present due to their selectivities less than 1%. Less than 6% selectivity of veratrole suggested that transalkylation was insignificant, which is in agreement with the results reported in the literature [11, 62]. Neither completely deoxygenated products (such as benzene and toluene) nor ring hydrogenation products

(such as cyclohexane, cyclohexene, cyclohexanone, etc.) were detected. High selectivity for phenol formation implied that the removal of the methoxy group was more favorable than the removal of the hydroxyl group of guaiacol in the alcohol solution. As no benzene was observed, the removal of the hydroxyl group to form benzene is more difficult and is not favorable when guaiacol is still present [33]. Based on the experimental results, possible reaction pathways for phenolic compounds production over Mo_2C@C are summarized in Fig. 10. Methyl substituents of cresols and xylenols were mainly formed through methyl-substitution from solvent rather than through transalkylation of guaiacol [63]. The comparative test was carried under the same condition in ethanol, and the main products were phenol, ethylphenols, and diethylphenols. This test proved that alkyl groups on cresols and xylenols were mainly from solvent *via* alky-substitution reactions. It is widely accepted that the selectivity of carbon supported catalysts is high, though their hydrogenation activities are lower than that of catalysts on acidic supports [15, 64]. Therefore, both the active metal Mo and the nature of the carbon support affected catalytic activities and determined the reaction pathway.

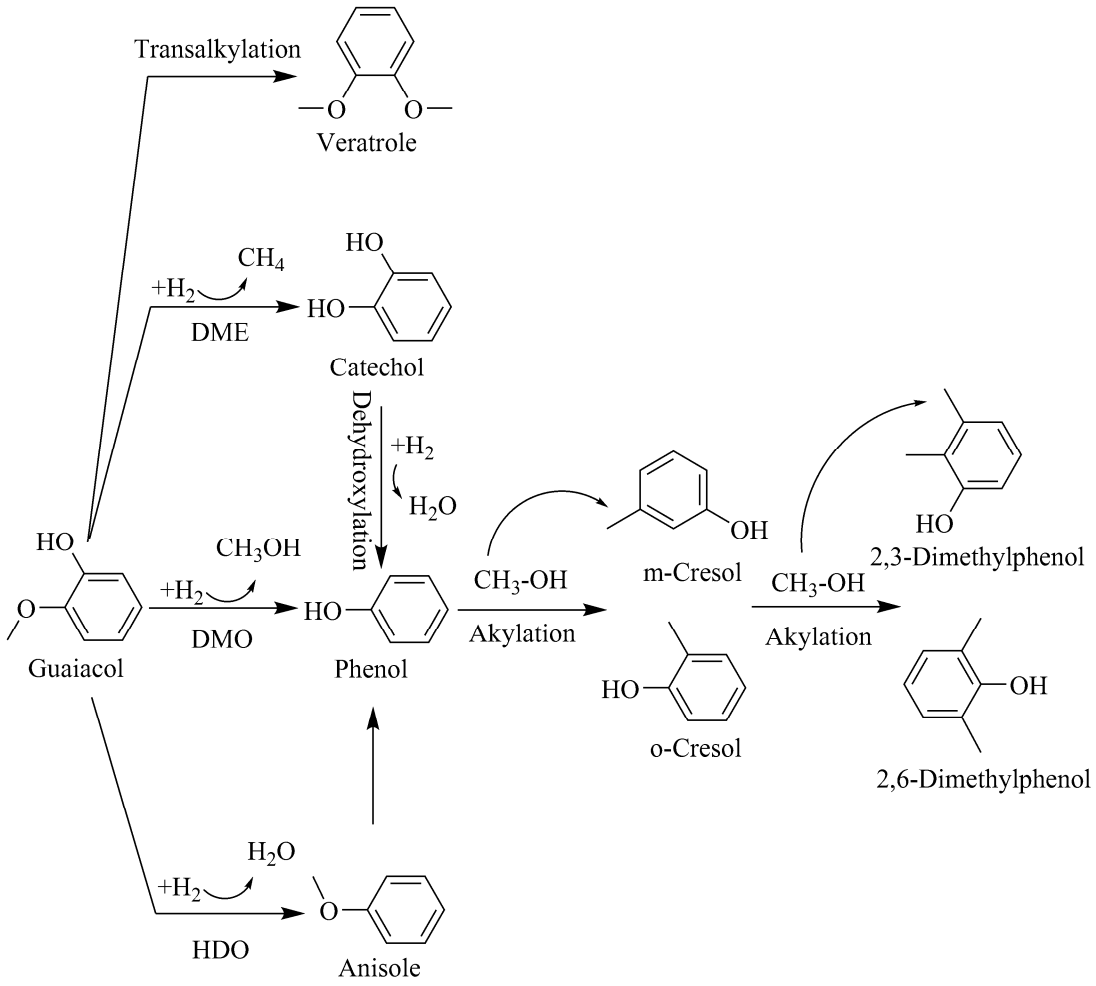

341

342 **Figure 10.** Proposed reaction pathway for guaiacol conversion over Mo_2C@C catalyst in

343 methanol.

344

345 **4. Conclusions**

346 The fabrication of highly dispersed molybdenum oxide nanoparticles embedded in

347 carbon nanospheres was achieved by one-pot hydrothermal carbonization of an

348 inexpensive precursor solution at a mild temperature. After TPRe, graphite encapsulated

349 molybdenum carbide Mo_2C@C was formed, which was composed of aggregates of

molybdenum core and carbon shell nanoparticles. The sizes of Mo_2C@C particles and molybdenum cores were 50-100 nm and 5-45 nm, respectively.

Mo_2C@C catalyst showed high selectivity to phenolic compounds in an alcohol solution, which exemplified the confining effect of the carbonaceous matrix to inhibit the aggregation of molybdenum nanoparticles during both the activation and reaction processes at a high temperature. The highest conversion efficiency and highest selectivities towards phenol and phenolics were obtained at 340°C under 2.8 MPa hydrogen pressure. Both demethoxylation and consecutive demethylation followed by a dehydroxylation proceeded concurrently to form phenol. Substitution of methyl or ethyl groups in phenol were from solvent methanol or ethanol. Moreover, no significant loss of catalytic activity even after three recycle times demonstrated that the core-shell structure of catalysts effectively offered the resistance to deactivation and sintering.

Acknowledgments

This work was supported by US-Department of Energy, Renewable Energy Center [award number: DE-EE0003138] and NSF-CREST Center for Bioenergy [Award No. HRD-1242152]. The HRTEM assistance of Dr. Yang Liu, in Analytical Instrumentation Facility at North Carolina State University supported by the State of North Carolina and the National Science Foundation, is gratefully acknowledged. The authors also thank Mr. Bryce M. Holmes and Mr. John R. Carver of Department of Natural Resources and Environmental Design, North Carolina A & T State University for using GC apparatus.

References

[1] C. Amen-Chen, H. Pakdel, C. Roy, Production of monomeric phenols by thermochemical conversion of biomass: a review, Bioresource Technology, 79 (2001) 277-299.
[2] P.M. Mortensen, J.D. Grunwaldt, P.A. Jensen, K.G. Knudsen, A.D. Jensen, A review of catalytic upgrading of bio-oil to engine fuels, Applied Catalysis A: General, 407 (2011) 1-19.
[3] G.W. Huber, S. Iborra, A. Corma, Synthesis of transportation fuels from biomass: chemistry, catalysts, and engineering, Chemical Reviews, 106 (2006) 4044-4098.
[4] D.C. Elliott, T.R. Hart, G.G. Neuenschwander, L.J. Rotness, A.H. Zacher, Catalytic hydroprocessing of biomass fast pyrolysis bio-oil to produce hydrocarbon products, Environmental Progress & Sustainable Energy, 28 (2009) 441-449.
[5] C. Yang, R. Li, C. Cui, S. Liu, Q. Qiu, Y. Ding, Y. Wu, B. Zhang, Catalytic hydroprocessing of microalgae-derived biofuels: a review, Green Chemistry, 18 (2016) 3684-3699.
[6] E. Santillan-Jimenez, M. Perdu, R. Pace, T. Morgan, M. Crocker, Activated Carbon, Carbon Nanofiber and Carbon Nanotube Supported Molybdenum Carbide Catalysts for the Hydrodeoxygenation of Guaiacol, Catalysts, 5 (2015) 424.
[7] D.C. Elliott, T.R. Hart, Catalytic Hydroprocessing of Chemical Models for Bio-oil, Energy & Fuels, 23 (2009) 631-637.
[8] P.E. Ruiz, K. Leiva, R. Garcia, P. Reyes, J.L.G. Fierro, N. Escalona, Relevance of sulfiding pretreatment on the performance of Re/ZrO2 and Re/ZrO2-sulfated catalysts for the hydrodeoxygenation of guayacol, Applied Catalysis A: General, 384 (2010) 78-83.
[9] Y.-C. Lin, C.-L. Li, H.-P. Wan, H.-T. Lee, C.-F. Liu, Catalytic Hydrodeoxygenation of Guaiacol on Rh-Based and Sulfided CoMo and NiMo Catalysts, Energy & Fuels, 25 (2011) 890-896.
[10] A. Gutierrez, R.K. Kaila, M.L. Honkela, R. Slioor, A.O.I. Krause, Hydrodeoxygenation of guaiacol on noble metal catalysts, Catalysis Today, 147 (2009) 239-246.
[11] T. Nimmanwudipong, R.C. Runnebaum, D.E. Block, B.C. Gates, Catalytic Conversion of Guaiacol Catalyzed by Platinum Supported on Alumina: Reaction Network Including Hydrodeoxygenation Reactions, Energy & Fuels, 25 (2011) 3417-3427.
[12] R. Runnebaum, T. Nimmanwudipong, R. Limbo, D. Block, B. Gates, Conversion of 4-Methylanisole Catalyzed by Pt/γ-Al2O3 and by Pt/SiO2-Al2O3: Reaction Networks and Evidence of Oxygen Removal, Catal Lett, 142 (2012) 7-15.
[13] M. Hellinger, H.W.P. Carvalho, S. Baier, D. Wang, W. Kleist, J.-D. Grunwaldt, Catalytic hydrodeoxygenation of guaiacol over platinum supported on metal oxides and zeolites, Applied Catalysis A: General, 490 (2015) 181-192.
[14] D. Gao, Y. Xiao, A. Varma, Guaiacol Hydrodeoxygenation over Platinum Catalyst: Reaction Pathways and Kinetics, Industrial & Engineering Chemistry Research, 54 (2015) 10638-10644.
[15] A.L. Jongerius, R. Jastrzebski, P.C.A. Bruijnincx, B.M. Weckhuysen, CoMo sulfide-catalyzed hydrodeoxygenation of lignin model compounds: An extended reaction

416 network for the conversion of monomeric and dimeric substrates, Journal of Catalysis,
417 285 (2012) 315-323.
418 [16] V.N. Bui, G. Toussaint, D. Laurenti, C. Mirodatos, C. Geantet, Co-processing of
419 pyrolisis bio oils and gas oil for new generation of bio-fuels: Hydrodeoxygenation of
420 guaïacol and SRGO mixed feed, Catalysis Today, 143 (2009) 172-178.
421 [17] V.N. Bui, D. Laurenti, P. Afanasiev, C. Geantet, Hydrodeoxygenation of guaiacol
422 with CoMo catalysts. Part I: Promoting effect of cobalt on HDO selectivity and activity,
423 Applied Catalysis B: Environmental, 101 (2011) 239-245.
424 [18] Z. He, X. Wang, Highly selective catalytic hydrodeoxygenation of guaiacol to
425 cyclohexane over Pt/TiO2 and NiMo/Al2O3 catalysts, Frontiers of Chemical Science and
426 Engineering, 8 (2014) 369-377.
427 [19] D.C. Elliott, Review of recent reports on process technology for thermochemical
428 conversion of whole algae to liquid fuels, Algal Research, 13 (2016) 255-263.
429 [20] C. Bouchy, C. Pham-Huu, B. Heinrich, C. Chaumont, M.J. Ledoux, Microstructure
430 and Characterization of a Highly Selective Catalyst for the Isomerization of Alkanes: A
431 Molybdenum Oxycarbide, Journal of Catalysis, 190 (2000) 92-103.
432 [21] L. Leclercq, K. Imura, S. Yoshida, T. Barbee, M. Boudart, Synthesis of New
433 Catalytic Materials: Metal Carbides of the Group VI B Elements, in: P.G.P.J. B. Delmon,
434 G. Poncelet (Eds.) Studies in Surface Science and Catalysis, Elsevier1979, pp. 627-639.
435 [22] M.-L. Frauwallner, F. López-Linares, J. Lara-Romero, C.E. Scott, V. Ali, E.
436 Hernández, P. Pereira-Almao, Toluene hydrogenation at low temperature using a
437 molybdenum carbide catalyst, Applied Catalysis A: General, 394 (2011) 62-70.
438 [23] H.C. Woo, K.Y. Park, Y.G. Kim, I.-S. Namau]Jong ShikChung, J.S. Lee, Mixed
439 alcohol synthesis from carbon monoxide and dihydrogen over potassium-promoted
440 molybdenum carbide catalysts, Applied Catalysis, 75 (1991) 267-280.
441 [24] A. Hynaux, C. Sayag, S. Suppan, J. Trawczynski, M. Lewandowski, A. Szymanska-
442 Kolasa, G. Djéga-Mariadassou, Kinetic study of the hydrodesulfurization of
443 dibenzothiophene over molybdenum carbides supported on functionalized carbon black
444 composite: Influence of indole, Applied Catalysis B: Environmental, 72 (2007) 62-70.
445 [25] P.A. Aegerter, W.W.C. Quigley, G.J. Simpson, D.D. Ziegler, J.W. Logan, K.R.
446 McCrea, S. Glazier, M.E. Bussell, Thiophene Hydrodesulfurization over Alumina-
447 Supported Molybdenum Carbide and Nitride Catalysts: Adsorption Sites, Catalytic
448 Activities, and Nature of the Active Surface, Journal of Catalysis, 164 (1996) 109-121.
449 [26] B. Diaz, S.J. Sawhill, D.H. Bale, R. Main, D.C. Phillips, S. Korlann, R. Self, M.E.
450 Bussell, Hydrodesulfurization over supported monometallic, bimetallic and promoted
451 carbide and nitride catalysts, Catalysis Today, 86 (2003) 191-209.
452 [27] A. Szymańska-Kolasa, M. Lewandowski, C. Sayag, D. Brodzki, G. Djéga-
453 Mariadassou, Comparison between tungsten carbide and molybdenum carbide for the
454 hydrodenitrogenation of carbazole, Catalysis Today, 119 (2007) 35-38.
455 [28] J. Han, J. Duan, P. Chen, H. Lou, X. Zheng, H. Hong, Nanostructured molybdenum
456 carbides supported on carbon nanotubes as efficient catalysts for one-step
457 hydrodeoxygenation and isomerization of vegetable oils, Green Chemistry, 13 (2011)
458 2561-2568.
459 [29] E. Furimsky, Metal carbides and nitrides as potential catalysts for hydroprocessing,
460 Applied Catalysis A: General, 240 (2003) 1-28.

[30] J. Han, J. Duan, P. Chen, H. Lou, X. Zheng, H. Hong, Carbon-Supported Molybdenum Carbide Catalysts for the Conversion of Vegetable Oils, ChemSusChem, 5 (2012) 727-733.
[31] W.-S. Lee, Z. Wang, W. Zheng, D.G. Vlachos, A. Bhan, Vapor phase hydrodeoxygenation of furfural to 2-methylfuran on molybdenum carbide catalysts, Catalysis Science & Technology, 4 (2014) 2340-2352.
[32] H. Ren, W. Yu, M. Salciccioli, Y. Chen, Y. Huang, K. Xiong, D.G. Vlachos, J.G. Chen, Selective Hydrodeoxygenation of Biomass-Derived Oxygenates to Unsaturated Hydrocarbons using Molybdenum Carbide Catalysts, ChemSusChem, 6 (2013) 798-801.
[33] A.L. Jongerius, R.W. Gosselink, J. Dijkstra, J.H. Bitter, P.C.A. Bruijnincx, B.M. Weckhuysen, Carbon Nanofiber Supported Transition-Metal Carbide Catalysts for the Hydrodeoxygenation of Guaiacol, ChemCatChem, 5 (2013) 2964-2972.
[34] R. Ma, K. Cui, L. Yang, X. Ma, Y. Li, Selective catalytic conversion of guaiacol to phenols over a molybdenum carbide catalyst, Chemical Communications, 51 (2015) 10299-10301.
[35] L. Volpe, M. Boudart, Compounds of molybdenum and tungsten with high specific surface area, Journal of Solid State Chemistry, 59 (1985) 348-356.
[36] S. Li, W.B. Kim, J.S. Lee, Effect of the Reactive Gas on the Solid-State Transformation of Molybdenum Trioxide to Carbides and Nitrides, Chemistry of materials, 10 (1998) 1853-1862.
[37] L. Hu, S. Ji, T. Xiao, C. Guo, P. Wu, P. Nie, Preparation and Characterization of Tungsten Carbide Confined in the Channels of SBA-15 Mesoporous Silica, The Journal of Physical Chemistry B, 111 (2007) 3599-3608.
[38] J.S. Lee, S.T. Oyama, M. Boudart, Molybdenum carbide catalysts, Journal of Catalysis, 106 (1987) 125-133.
[39] J.B. Claridge, A.P.E. York, A.J. Brungs, M.L.H. Green, Study of the Temperature-Programmed Reaction Synthesis of Early Transition Metal Carbide and Nitride Catalyst Materials from Oxide Precursors, Chemistry of materials, 12 (2000) 132-142.
[40] A. Hanif, T. Xiao, A.P.E. York, J. Sloan, M.L.H. Green, Study on the Structure and Formation Mechanism of Molybdenum Carbides, Chemistry of Materials, 14 (2002) 1009-1015.
[41] T.H. Nguyen, T.V. Nguyen, Y.J. Lee, T. Safinski, A.A. Adesina, Structural evolution of alumina supported Mo–W carbide nanoparticles synthesized by precipitation from homogeneous solution, Materials Research Bulletin, 40 (2005) 149-157.
[42] X.-H. Wang, H.-L. Hao, M.-H. Zhang, W. Li, K.-Y. Tao, Synthesis and characterization of molybdenum carbides using propane as carbon source, Journal of Solid State Chemistry, 179 (2006) 538-543.
[43] T.-c. Xiao, A.P.E. York, V.C. Williams, H. Al-Megren, A. Hanif, X.-y. Zhou, M.L.H. Green, Preparation of Molybdenum Carbides Using Butane and Their Catalytic Performance, Chemistry of materials, 12 (2000) 3896-3905.
[44] Q. Wang, H. Li, L. Chen, X. Huang, Monodispersed hard carbon spherules with uniform nanopores, Carbon, 39 (2001) 2211-2214.
[45] G. Yu, B. Sun, Y. Pei, S. Xie, S. Yan, M. Qiao, K. Fan, X. Zhang, B. Zong, FexOy@C Spheres as an Excellent Catalyst for Fischer−Tropsch Synthesis, Journal of the American Chemical Society, 132 (2010) 935-937.

[46] L. She, J. Li, Y. Wan, X. Yao, B. Tu, D. Zhao, Synthesis of ordered mesoporous MgO/carbon composites by a one-pot assembly of amphiphilic triblock copolymers, Journal of Materials Chemistry, 21 (2011) 795-800.
[47] J. Dou, H.C. Zeng, Preparation of Mo-Embedded Mesoporous Carbon Microspheres for Friedel–Crafts Alkylation, The Journal of Physical Chemistry C, 116 (2012) 7767-7775.
[48] C. Avendano, A. Briceno, F.J. Mendez, J.L. Brito, G. Gonzalez, E. Canizales, R. Atencio, P. Dieudonne, Novel MoO2/carbon hierarchical nano/microcomposites: synthesis, characterization, solid state transformations and thiophene HDS activity, Dalton Transactions, 42 (2013) 2822-2830.
[49] W. Wang, G. Ding, T. Jiang, P. Zhang, T. Wu, B. Han, Facile one-pot synthesis of VxOy@C catalysts using sucrose for the direct hydroxylation of benzene to phenol, Green Chemistry, 15 (2013) 1150-1154.
[50] C. Liu, M. Lin, K. Fang, Y. Meng, Y. Sun, Preparation of nanostructured molybdenum carbides for CO hydrogenation, RSC Advances, 4 (2014) 20948-20954.
[51] C.O. Tuck, E. Pérez, I.T. Horváth, R.A. Sheldon, M. Poliakoff, Valorization of Biomass: Deriving More Value from Waste, Science, 337 (2012) 695-699.
[52] R. Ma, W. Hao, X. Ma, Y. Tian, Y. Li, Catalytic Ethanolysis of Kraft Lignin into High-Value Small-Molecular Chemicals over a Nanostructured α-Molybdenum Carbide Catalyst, Angewandte Chemie International Edition, 53 (2014) 7310-7315.
[53] X. Sun, Y. Li, Colloidal Carbon Spheres and Their Core/Shell Structures with Noble-Metal Nanoparticles, Angewandte Chemie International Edition, 43 (2004) 597-601.
[54] T.P. St. Clair, B. Dhandapani, S.T. Oyama, Cumene hydrogenation turnover rates on Mo2C: CO and O2 as probes of the active site, Catal Lett, 58 (1999) 169-171.
[55] M. Sevilla, A.B. Fuertes, Chemical and Structural Properties of Carbonaceous Products Obtained by Hydrothermal Carbonization of Saccharides, Chemistry – A European Journal, 15 (2009) 4195-4203.
[56] M.-M. Titirici, M. Antonietti, Chemistry and materials options of sustainable carbon materials made by hydrothermal carbonization, Chemical Society Reviews, 39 (2010) 103-116.
[57] R. Li, A. Shahbazi, A Review of Hydrothermal Carbonization of Carbohydrates for Carbon Spheres Preparation, Trends in Renewable Energy, 1 (2015) 43-56.
[58] Y. Qi, M. Zhang, L. Qi, Y. Qi, Mechanism for the formation and growth of carbonaceous spheres from sucrose by hydrothermal carbonization, RSC Advances, 6 (2016) 20814-20823.
[59] M.D. Bazhenova, N.N. Gavrilova, V.V. Nazarov, Some colloidochemical properties of molybdenum blues synthesized using glucose as a reducing agent, Colloid Journal, 77 (2015) 1-5.
[60] V.K. LaMer, R.H. Dinegar, Theory, Production and Mechanism of Formation of Monodispersed Hydrosols, Journal of the American Chemical Society, 72 (1950) 4847-4854.
[61] J. Besnardiere, X. Petrissans, C. Surcin, V. Buissette, T. Le Mercier, M. Morcrette, D. Portehault, S. Cassaignon, Sustainable one-pot aqueous route to hierarchical carbon-MoO2 electrodes for Li-ion batteries, RSC Advances, 4 (2014) 21208-21215.

551 [62] C.-J. Chen, W.-S. Lee, A. Bhan, Mo2C catalyzed vapor phase hydrodeoxygenation
552 of lignin-derived phenolic compound mixtures to aromatics under ambient pressure,
553 Applied Catalysis A: General, 510 (2016) 42-48.
554 [63] J.E. Peters, J.R. Carpenter, D.C. Dayton, Anisole and Guaiacol Hydrodeoxygenation
555 Reaction Pathways over Selected Catalysts, Energy & Fuels, 29 (2015) 909-916.
556 [64] R. Olcese, M.M. Bettahar, B. Malaman, J. Ghanbaja, L. Tibavizco, D. Petitjean, A.
557 Dufour, Gas-phase hydrodeoxygenation of guaiacol over iron-based catalysts. Effect of
558 gases composition, iron load and supports (silica and activated carbon), Applied Catalysis
559 B: Environmental, 129 (2013) 528-538.

560